Nanoscale Advances

ROYAL SOCIETY OF CHEMISTRY

PAPER

View Article Online
View Journal | View Issue

Cite this: *Nanoscale Adv.*, 2025, **7**, 4852

A nanomagnetic triazole-based Schiff-base complex of palladium(0) as an efficient heterogeneous catalyst for the Mizoroki–Heck C–C cross-coupling reaction under green conditions

Yassin T. H. Mehdar, *[a] Fatimah Mohammed Alshamsan,[b] Asma Ahmad Nashawi,[c] Hussein Eledum,[d] Ahmed Mohajja Alshammari[e] and Jawza A. Almutairi[f]

Received 16th April 2025
Accepted 29th May 2025

DOI: 10.1039/d5na00364d

rsc.li/nanoscale-advances

A novel magnetically recoverable palladium(0) catalyst, [Fe_3O_4@triazole-Schiff-base-Pd(0)], was synthesized *via* a simple three-step functionalization. Magnetite nanoparticles were first modified with a haloalkane silane linker to introduce C–Cl functionalities, followed by nucleophilic substitution with a triazole-Schiff-base ligand derived from 3-amino-1,2,4-triazole and salicylaldehyde. Finally, coordination with palladium chloride and *in situ* reduction to Pd(0) afforded a stable, magnetically separable catalyst. Comprehensive characterization (FT-IR, XRD, TGA, EDX, ICP-OES, WDX, FE-SEM, TEM, and VSM) confirmed its successful synthesis. The catalyst demonstrated outstanding activity in the Mizoroki–Heck C–C cross-coupling reaction, resulting in efficient coupling of a diverse range of aryl iodides, bromides, and chlorides with butyl acrylate in PEG-400 as a green solvent and co-catalyst. It exhibited superior selectivity for aryl iodides and bromides and maintained high efficiency over eight consecutive cycles with minimal metal leaching. The use of cost-effective materials, facile magnetic recovery, and scalability make this catalyst an eco-friendly and economically viable alternative to conventional palladium-based methodologies.

1 Introduction

The Heck cross-coupling reaction, a pivotal tool in modern organic synthesis, facilitates the formation of carbon–carbon bonds *via* the palladium-catalyzed coupling of aryl or vinyl halides with alkenes.[1] This reaction was initially developed by Richard F. Heck in the late 1960s and later recognized with the 2010 Nobel Prize in Chemistry, and this synthetic tool has become indispensable in the production of pharmaceuticals, agrochemicals, and advanced materials.[2,3] Despite the well-established efficiency and selectivity of homogeneous palladium catalysts with phosphine ligands, significant challenges remain, including catalyst recovery, metal leaching, ligand cost, and alkene stability issues.[4–9] A significant hurdle lies in the practical handling of the alkene reactants. Olefins used in Heck coupling pose challenges, including difficulties in synthesis and purification, as well as a tendency to polymerize during storage or at high reaction temperatures. Even commercially available alkenes often require excess amounts to counteract these stability issues.[10,11] This, coupled with concerns regarding residual palladium contamination, has spurred significant research. Current efforts are focused on the development of heterogeneous catalysts, including those supported on zeolites, metal oxides and polymeric frameworks, and the application of palladium nanoparticles.[8,12–14] These advancements aim to enhance sustainability and recyclability, and mitigate the challenges associated with alkene instability, broadening the industrial applicability of the Heck reaction and ensuring its continued relevance in contemporary chemical research and production.[14–16]

To improve sustainability and economic efficiency, heterogeneous catalysis has emerged as a compelling alternative to traditional homogeneous methods.[17] The inherent advantages of heterogeneous systems, notably enhanced recyclability and selectivity, are largely attributed to the strategic use of solid

[a]*Department of Chemistry, Taibah University, P. O. Box 30002, Al-Madinah *Al-Munawwarah*, 14177, Saudi Arabia. E-mail: yassinthmehdar@gmail.com; ymehdar@taibahu.edu.sa*

[b]*Department of Food Sciences and Nutrition, College of Food and Agricultural Sciences, King Saud University, P. O. Box 2460, Riyadh 11451, Saudi Arabia. E-mail: Falshamsan@ksu.edu.sa*

[c]*Department Faculty of Pharmacy, University King Abdulaziz University, Jeddah, Saudi Arabia*

[d]*Department of Statistics, University of Tabuk, Tabuk, Saudi Arabia*

[e]*Department of Biology, College of Science, University of Ha'il, P. O. Box 2440, Ha'il, Saudi Arabia*

[f]*College of Pharmacy, Pharmaceutical Science, Princess Nourah Bint Abdulrahman University, Riyadh, Saudi Arabia. E-mail: Jawza.a.almutairi@gmail.com*

supports that anchor active catalytic species.[18] Among various catalytic supports, magnetic metal oxide nanoparticles, particularly spinel ferrites, have gained significant attention due to their unique combination of catalytic activity, stability, and ease of recovery.[19] Within this class, magnetic metal oxide nanoparticles, particularly spinel ferrites, have garnered significant attention as exceptionally effective catalytic supports.[20,21] They uniquely combine the benefits of green catalytic activity with the practical advantages of facile magnetic separation, high stability, and reusability, thereby streamlining catalyst recovery and significantly reducing waste generation across various applications.[22] Among these, Fe_3O_4 stands out for its widespread adoption, balancing magnetic separability with excellent catalytic support properties. Crucially, the surface hydroxyl groups present on Fe_3O_4 nanoparticles offer a versatile platform for effective functionalization through chemical bonding, enabling the tailored design of catalysts for specific applications.[23,24]

To further enhance catalytic performance, Schiff-base ligands, formed by condensing amines and carbonyls, have been explored due to their ability to form stable metal complexes. Their applications include biological studies, materials science, and catalysis, where they exhibit significant activity and stabilize various metal oxidation states.[25–27] While the convenient synthesis and solvent compatibility of these ligands drive their catalytic utility, the immobilization of these ligands on solid supports, though a burgeoning field, continues to demand novel strategies and refined methodologies for enhanced performance.[28–30]

This study aims to overcome key limitations of traditional Heck catalysts including high costs, environmental concerns, and catalyst recovery issues by developing a novel immobilization strategy using chlorine-functionalized Fe_3O_4 MNPs. This study employs chlorine-functionalized Fe_3O_4 MNPs as a stable, cost-effective support for a triazole-Schiff-base ligand derived from 3-amino-1,2,4-triazole and salicylaldehyde, along with its corresponding palladium(0) complex. This approach yields a magnetically recoverable, low-cost, and environmentally benign palladium catalyst designed to facilitate Heck coupling reactions under mild, sustainable conditions. By leveraging the unique properties of MNPs, we aim to demonstrate enhanced catalyst stability, recyclability, and activity. Furthermore, this study will investigate the catalyst's performance across a range of substrates, exploring its scope and limitations.

2 Experimental

2.1. Typical procedure for synthesis of the [Fe_3O_4@triazole-Schiff-base-Pd(0)] complex

Fe_3O_4 MNPs were synthesized according to a previously reported method.[31] Subsequently, 10 g of the Fe_3O_4 MNPs were dispersed in 200 mL of anhydrous toluene and sonicated for 1 h. 20 mL of (3-chloropropyl)trimethoxysilane (CPTMS) was then added dropwise to the vigorously stirred suspension. The resulting mixture was heated to 80 °C and stirred for 48 h. After the reaction, the Fe3O4@CPTMS MNPs were magnetically separated, washed with *n*-hexane, and dried under vacuum at 80 °C overnight. In the subsequent step, 5 g of the Fe_3O_4@-CPTMS MNPs were dispersed in 150 mL of anhydrous acetonitrile and sonicated for 1 h to afford a homogeneous suspension. A solution of 3-amino-1,2,4-triazole Schiff-base (prepared by reacting equimolar amounts (10 mmol) of 3-amino-1,2,4-triazole and salicylaldehyde in acetonitrile (25 mL) under reflux conditions for 4 h (ref. 32–34)) and 5 mmol of anhydrous K_2CO_3 were added to the Fe_3O_4@CPTMS MNP suspension. The reaction mixture was stirred under reflux

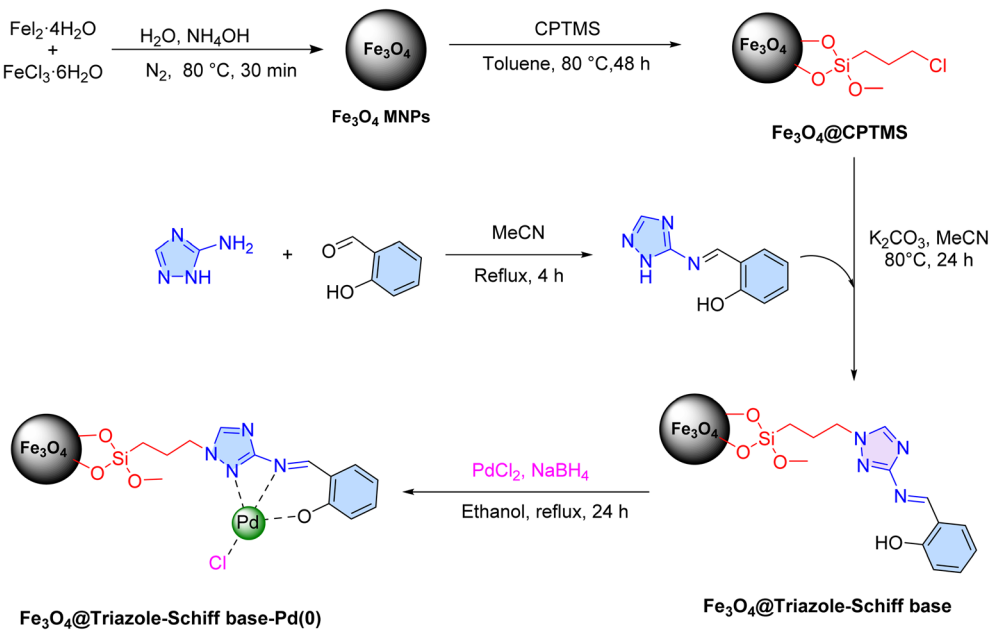

Scheme 1 Stepwise synthesis of the [Fe_3O_4@triazole-Schiff-base-Pd(0)] catalyst.

conditions under a nitrogen atmosphere for 24 h. The resulting Fe_3O_4@triazole-Schiff-base product was magnetically separated, washed with hot ethanol, and dried at 80 °C for 4 h. Finally, 2 g of Fe_3O_4@triazole-Schiff-base was dispersed in 100 mL of ethanol and stirred for 30 minutes. 4 mmol of $PdCl_2$ was then added to this suspension, and the mixture was refluxed for 20 h. Finally the reaction mixture was cooled to room temperature and 10 mmol of $NaBH_4$ was added to the reaction and refluxed for an additional 4 h. The resulting [Fe_3O_4@triazole-Schiff-base-Pd(0)] complex was magnetically separated, washed sequentially with hot deionized water and ethanol, and dried at 80 °C for 6 h.

2.2. General procedure for the Mizoroki–Heck reaction catalyzed by [Fe_3O_4@triazole-Schiff-base-Pd(0)]

In a reaction vessel, a mixture of an aryl halide (1 mmol), an alkene (1 mmol), potassium carbonate (3 mmol), and a [Fe_3O_4@triazole-Schiff-base-Pd(0)] catalyst (5 mg) was suspended in 3 mL of polyethylene glycol (PEG-400). The reaction was stirred at 100 °C until complete, with progress tracked by thin-layer chromatography (TLC). Upon completion, the reaction mixture was diluted with hot water, the catalyst was separated by using a magnetic field and the product was extracted into ethyl acetate and washed with warm water. The organic extract was dried over sodium sulfate and filtered. After rotary evaporation to remove the solvent, the crude butyl cinnamate product was subjected to preparative silica gel TLC for purification.

3 Results and discussion

In this study, a novel palladium triazole-Schiff-base complex was successfully grafted onto Fe_3O_4 MNPs through a three-step post-synthetic functionalization protocol. This process was initiated with the synthesis and surface modification of Fe_3O_4 MNPs using the CPTMS linker, introducing reactive chloropropyl functionalities. Subsequently, an *in situ* generated 3-amino-1,2,4-triazole Schiff-base ligand was used to perform a nucleophilic substitution reaction on this substrate. This

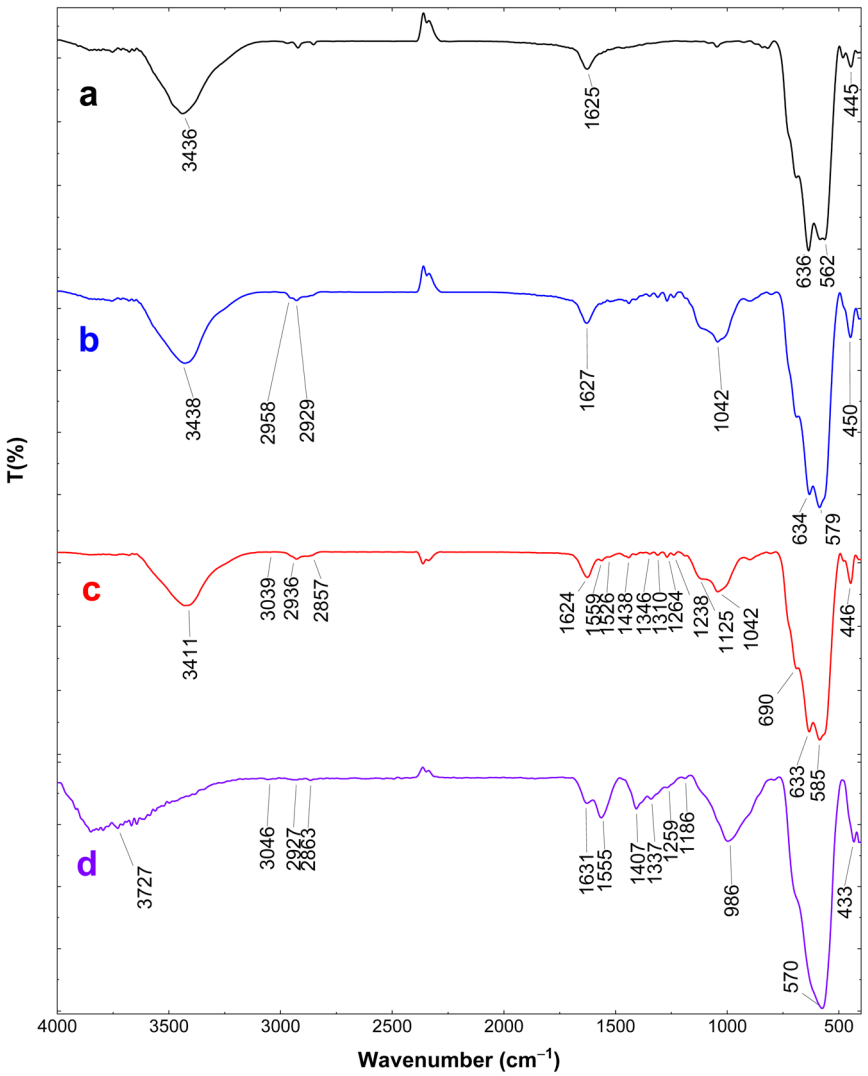

Fig. 1 FT-IR spectra of (a) Fe_3O_4, (b) Fe_3O_4@CPTMS (c) Fe_3O_4@triazole-Schiff-base and (d) [Fe_3O_4@triazole-Schiff-base-Pd(0)].

ligand was synthesized *via* a condensation reaction (Hoeg's reaction) between 3-amino-1,2,4-triazole and salicylaldehyde. Finally, the immobilized Schiff-base ligand was complexed with palladium(II) chloride, followed by *in situ* reduction with $NaBH_4$ to generate the [Fe_3O_4@triazole-Schiff-base-Pd(0)] catalyst (Scheme 1). The synthesis and immobilization of the targeted catalytic complex were rigorously characterized using a series of analytical techniques, including Fourier-transform infrared spectroscopy (FT-IR), X-ray diffraction (XRD), thermogravimetric analysis (TGA), energy-dispersive X-ray spectroscopy (EDX), inductively coupled plasma optical emission spectrometry (ICP-OES), elemental mapping, field-emission scanning electron microscopy (FE-SEM), transmission electron microscopy (TEM), and vibrating sample magnetometry (VSM) to comprehensively evaluate its structural, compositional, and magnetic properties.

3.1. Catalyst characterization

The FTIR spectra of pristine Fe_3O_4, Fe_3O_4@CPTMS, Fe_3O_4@-triazole-Schiff-base, and the [Fe_3O_4@triazole-Schiff-base-Pd(0)] catalyst are shown in Fig. 1. The FTIR spectrum of pristine Fe_3O_4 exhibits an Fe–O stretching band at 562 cm^{-1}. Broad peaks at 3436 cm^{-1} and 1625 cm^{-1} correspond to O–H bond vibrations from hydroxyl groups on the Fe_3O_4 surface.[35] In the spectrum of Fe_3O_4@CPTMS, additional peaks at 1042 cm^{-1} and 2929 cm^{-1} are attributed to the Si–O–Si stretching vibrations and aliphatic C–H bonds, respectively, confirming the successful functionalization with CPTMS.[36] The FTIR spectrum of Fe_3O_4@triazole-Schiff-base shows new peaks at 1438, 1559, and 1624 cm^{-1}, which are assigned to the aromatic C–C and C=N stretching vibrations in the Schiff base and triazole ring.[33] These peaks further support the successful immobilization of the Schiff base ligand onto the haloalkene-modified magnetic support. Finally, the FTIR spectrum of the [Fe_3O_4@triazole-Schiff-base-Pd(0)] catalyst reveals several changes such as some shifts in the C=N and N–H peaks, likely due to the π-back-bonding effect of the immobilized Pd(0) ions, confirming the formation of the targeted catalyst.

Powder X-ray diffraction (P-XRD) was employed to characterize the crystalline phases present in the [Fe_3O_4@triazole-Schiff-base-Pd(0)] catalyst. The diffraction pattern exhibited sharp reflections at 2θ values of 30.10°, 35.24°, 43.05°, 53.75°, 57.14°, and 62.83°, which correspond to the (220), (311), (400), (422), (511), and (440) crystallographic planes of cubic Fe_3O_4, consistent with JCPDS 88-0866.[37] This confirmed the formation and stability of the magnetite nanoparticles during the multi-step synthetic procedure. Furthermore, reflections at 2θ values of 37.52°, 45.44°, 50.14°, and 65.02° were attributed to metallic Pd(0),[38] indicating the successful incorporation of palladium within the catalyst structure. Additionally, the approximate crystallite size calculated from the (311) peak using the Debye–Scherrer equation is about 15.2 nm (Fig. 2).

The thermal behavior of the [Fe_3O_4@triazole-Schiff-base-Pd(0)] catalyst was evaluated *via* the TGA technique, as shown in Fig. 3. The TGA curve reveals an initial weight loss of approximately 4.9% in the temperature range of 25–200 °C, attributed to the evaporation of physically and chemically adsorbed moisture and organic solvents. A significant weight loss of around 29% occurs between 200 °C and 600 °C, corresponding to the decomposition of the supported organic components, including the CPTMS linker and Schiff-base ligand, through pyrolysis reactions involving oxygen, heat and the hydrocarbon. These results confirm the presence of organic moieties on the catalyst surface and indicate its thermal stability up to 200 °C, making it suitable for reactions conducted at temperatures below this threshold.

The elemental composition of the [Fe_3O_4@triazole-Schiff-base-Pd(0)] catalyst was investigated using energy dispersive spectroscopy (EDS) (Fig. 4). The presence of characteristic signals for iron (40.38 wt%, 20.58 at%) and oxygen (19.63 wt%, 34.93 at%) confirmed the incorporation of iron oxide magnetic nanoparticles within the composite matrix. The detection of silicon (1.66 wt%, 1.68 at%) validated the successful silane coating and attachment of the CPTMS linker to the support. Carbon (12.37 wt%, 29.30 at%) and nitrogen (3.58 wt%, 7.27 at%) signals also provided evidence for successful surface

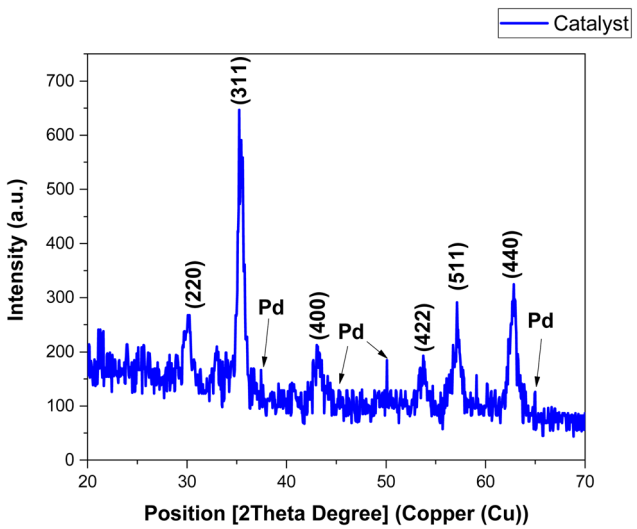

Fig. 2 XRD pattern of the [Fe_3O_4@triazole-Schiff-base-Pd(0)] catalyst.

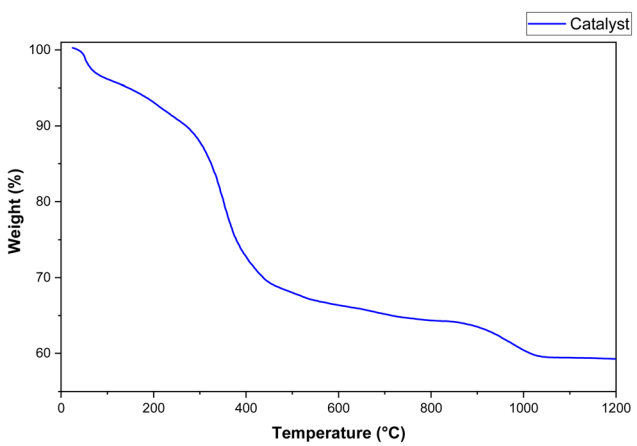

Fig. 3 TGA curve of the [Fe_3O_4@triazole-Schiff-base-Pd(0)] catalyst.

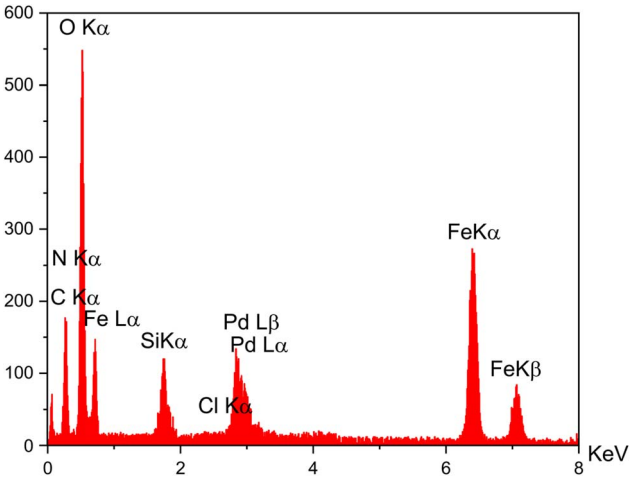

Fig. 4 EDX analysis of the [Fe_3O_4@triazole-Schiff-base-Pd(0)] catalyst.

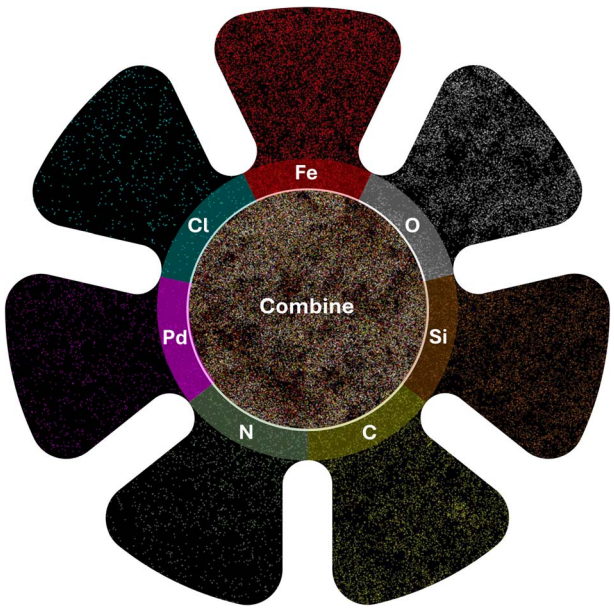

Fig. 5 EDX elemental mapping images of the [Fe_3O_4@triazole-Schiff-base-Pd(0)] catalyst.

functionalization with the CPTMS linker and the triazole-Schiff-base ligand. Finally, the presence of palladium (15.87 wt%, 4.25 at%) and chlorine (2.51 wt%, 2.02 at%) signals demonstrated the effective coordination of palladium chloride to the surface-bound ligands, confirming the synthesis of the desired palladium catalytic complex. The concentration of palladium within the [Fe_3O_4@triazole-Schiff-base-Pd(0)] catalyst, as determined by ICP-OES, was measured to be 1.67×10^{-3} mol g^{-1}.

Elemental mapping of the [Fe_3O_4@triazole-Schiff-base-Pd(0)] catalyst demonstrated a high surface density of iron and oxygen, consistent with the Fe_3O_4 core (Fig. 5). The homogeneous distribution of silicon, carbon, and nitrogen confirmed the uniform coverage of the silane linker and further Schiff-base ligand immobilization. Furthermore, the homogeneous dispersion of palladium and chlorine provided evidence for the accessibility of the active catalytic species across the nanoparticle surface. These results confirm the successful functionalization of Fe_3O_4 MNPs and formation of the [Fe_3O_4@triazole-Schiff-base-Pd(0)] catalyst.

The morphology of the [Fe_3O_4@triazole-Schiff-base-Pd(0)] catalyst was characterized using SEM and TEM analysis, as shown in Fig. 6. The SEM image (Fig. 6a) demonstrates that the catalyst particles exhibit a quasi-spherical shape with uniform dispersion, which is consistent with the typical morphology of magnetic nanoparticles reported in the literature. This observation further substantiates the stability of the catalytic support throughout the post-synthetic modification process.[39] However, some agglomeration was also observed, which can be attributed to the intrinsic magnetic properties of Fe_3O_4 and the surface modification with polar groups. This agglomeration is indicative of successful catalyst synthesis, confirming the effectiveness of the synthesis method and the integrity of the catalyst structure. The TEM micrographs clearly show that the spherical shape particles are uniformly distributed with good dispersion, ranging from 15 to 20 nm in size. Additionally, the lighter layer of supported groups around the darker Fe_3O_4 core is clearly visible, confirming the successful immobilization of the targeted complex onto the MNP support (Fig. 6b).

The magnetic behavior of the [Fe_3O_4@triazole-Schiff-base-Pd(0)] catalyst was characterized at ambient temperature *via*

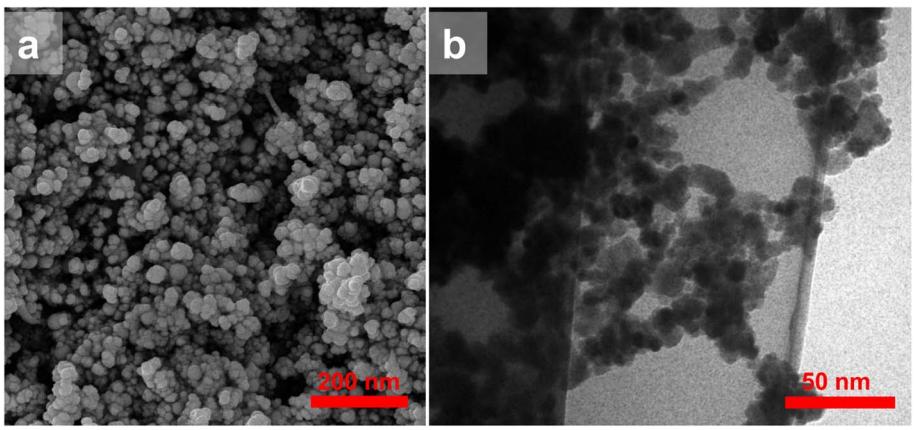

Fig. 6 (a) SEM and (b) TEM images of the [Fe_3O_4@triazole-Schiff-base-Pd(0)] catalyst.

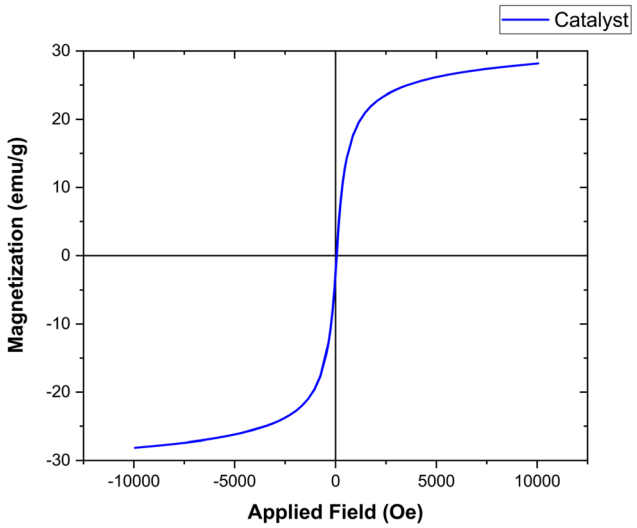

Fig. 7 VSM analysis of the [Fe_3O_4@triazole-Schiff-base-Pd(0)] catalyst.

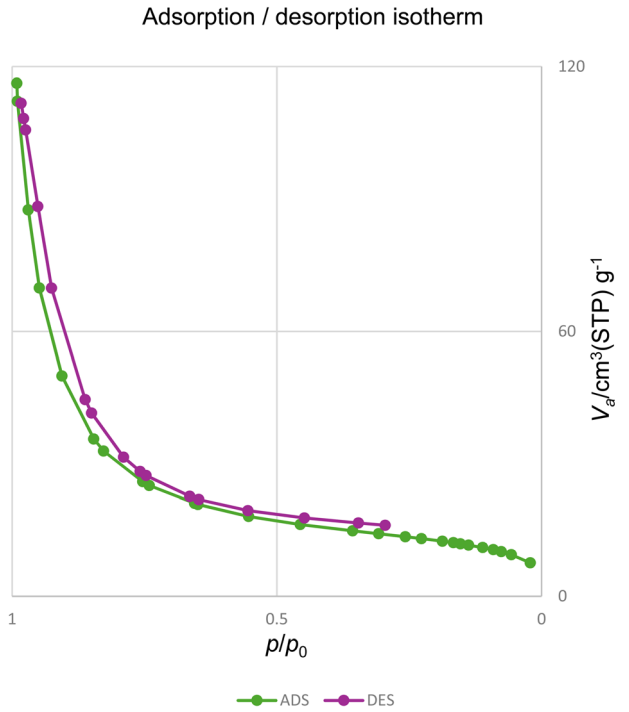

Fig. 8 VSM analysis of the [Fe_3O_4@triazole-Schiff-base-Pd(0)] catalyst.

vibrating sample magnetometry (VSM). The obtained hysteresis loop (Fig. 7) revealed a ferromagnetic response with a saturation magnetization (M_s) of approximately 28 emu g^{-1}. This value represents a decrease compared to the higher M_s values reported for unmodified Fe_3O_4.[40] This decrement is attributed to the presence of the non-magnetic moieties, which effectively decrease the overall magnetic moment per unit mass of the composite material, providing evidence of successful surface functionalization with the [triazole-Schiff-base-Pd(0)] complex. Nonetheless, the catalyst exhibited sufficient magnetic properties to enable efficient magnetic separation from reaction media using an external magnetic field.

The nitrogen adsorption–desorption isotherm of the [Fe_3O_4@triazole-Schiff-base-Pd(0)] complex was a type IV isotherm according to the IUPAC classification, accompanied by an H3-type hysteresis loop (Fig. 8). The Brunauer–Emmett–Teller (BET) specific surface area was determined to be 56.36 m^2 g^{-1}, and the average pore diameter was calculated to be 17.33 nm, unequivocally confirming the mesoporous nature of the material. Furthermore, the total pore volume (V_p) was found to be 0.115 cm^3 g^{-1}, suggesting a substantial pore network capable of facilitating the efficient diffusion of reactants and products during catalytic applications.

3.2. Catalytic study

After the complete characterization of [Fe_3O_4@triazole-Schiff-base-Pd(0)] its catalytic efficiency was examined in the Mizoroki–Heck C–C coupling reaction of aryl halides and butyl acrylate as an industrially important reaction. For this purpose initially the coupling of iodobenzene and butyl acrylate was selected as a model reaction to optimize reaction parameters, including the catalyst amount, solvent, base type and reaction temperature (Table 1). Initially, we conducted the reaction under catalyst free conditions, but after 1 day no product was observed (Table 1, entry 1). Then the catalytic activity of Fe_3O_4, Fe_3O_4@CPTMS and Fe_3O_4@triazole-Schiff-base MNPs was investigated, but in this case as monitored by TLC no detectable product was formed even after 4 h (Table 1, entries 2–4). But when the reaction was conducted in the presence of [Fe_3O_4@-triazole-Schiff-base-Pd(0)] MNPs reaction progress was observed but the catalytic efficiency was observed to be quite low (35%) when the reaction was performed using 1 mg of the catalyst (Table 1, entry 5). So the reaction was conducted by varying the catalyst amounts from 1–6 mg, resulting in enhanced yields of the coupling reaction (Table 1, entries 5–9). The evaluation determined that using 5 mg of the catalyst is the most appropriate catalytic amount for the per 1 mmol scale reaction with 98% yield (Table 1, entry 8). Furthermore, increasing the catalyst loading to 6 mg did not result in improved yields or reaction time (Table 1, entry 9).

Then the effect of more green solvents including water and ethanol; however, the outcomes were unsatisfactory and these solvents led to a decrement in the reaction efficiency, so PEG-400 was used as the optimal solvent. Then an investigation was conducted to optimize the alkaline media of the reaction, and base-free conditions and several bases including; K_2CO_3, Na_2CO_3, KOH and organic triethylamine base were tested (Table 1, entries 8 and 12–15). Furthermore, in the absence of a base, only a trace amount of product was obtained (Table 1, entry 12). Additionally, reducing the base amount from 3 mmol to 1 mmol resulted in a decrease in yield, while increasing it to 4 mmol produced similar results to 3 mmol (Table 1, entries 18 and 19). Among the tested bases, 3 mmol of K_2CO_3 provided the best efficiency, making it the optimal base for this coupling reaction methodology (Table 1, entry 8). Furthermore, the optimal conditions were found to be 5 mg of the [Fe_3O_4@triazole-Schiff-

Table 1 Optimization of synthesis of butyl cinnamate *via* the Mizoroki–Heck reaction of iodobenzene and butyl acrylate in the presence of the [Fe_3O_4@triazole-Schiff-base-Pd(0)] catalyst

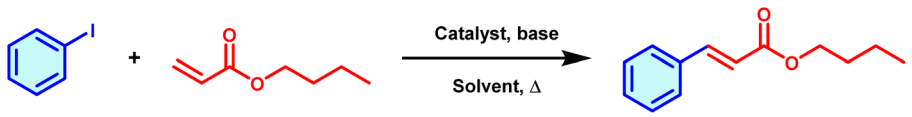

Entry	Catalyst	Catalyst amount (mg)	Base	Solvent	Temperature (°C)	Time (min)	Yield[a,b] (%)
1	—	—	K_2CO_3	PEG-400	120	1 day	NR
2	Fe_3O_4	5	K_2CO_3	PEG-400	120	4 h	NR
3	Fe_3O_4@CPTMS	5	K_2CO_3	PEG-400	120	4 h	NR
4	Fe_3O_4@triazole-Schiff-base	5	K_2CO_3	PEG-400	120	4 h	NR
5	[Fe_3O_4@triazole-Schiff-base-Pd(0)]	1	K_2CO_3	PEG-400	120	25	35
6	[Fe_3O_4@triazole-Schiff-base-Pd(0)]	3	K_2CO_3	PEG-400	120	25	87
7	[Fe_3O_4@triazole-Schiff-base-Pd(0)]	4	K_2CO_3	PEG-400	120	25	95
8	[Fe_3O_4@triazole-Schiff-base-Pd(0)]	5	K_2CO_3	PEG-400	120	25	98
9	[Fe_3O_4@triazole-Schiff-base-Pd(0)]	6	K_2CO_3	PEG-400	120	25	98
10	[Fe_3O_4@triazole-Schiff-base-Pd(0)]	5	K_2CO_3	Water	Reflux	180	78
11	[Fe_3O_4@triazole-Schiff-base-Pd(0)]	5	K_2CO_3	Ethanol	Reflux	135	93
12	[Fe_3O_4@triazole-Schiff-base-Pd(0)]	5	—	PEG-400	80	2 h	Trace
13	[Fe_3O_4@triazole-Schiff-base-Pd(0)]	5	Na_2CO_3	PEG-400	80	2 h	95
14	[Fe_3O_4@triazole-Schiff-base-Pd(0)]	5	KOH	PEG-400	120	25	49
15	[Fe_3O_4@triazole-Schiff-base-Pd(0)]	5	Et_3N	PEG-400	120	25	93
16	[Fe_3O_4@triazole-Schiff-base-Pd(0)]	5	K_2CO_3	PEG-400	60	25	47
17	[Fe_3O_4@triazole-Schiff-base-Pd(0)]	5	K_2CO_3	PEG-400	r.t.	25	Trace
18	[Fe_3O_4@triazole-Schiff-base-Pd(0)]	5	K_2CO_3 (1 mmol)	PEG-400	120	25	87
19	[Fe_3O_4@triazole-Schiff-base-Pd(0)]	5	K_2CO_3 (4 mmol)	PEG-400	120	25	98

[a] Isolated yield. [b] Conditions: iodobenzene (1 mmol), butyl acrylate (1 mmol), base (3 mmol), catalyst (mg) and solvent (3 mL).

base-Pd(0)] nanocatalyst and K_2CO_3 (3 mmol) in PEG-400 at 120 C (Table 1 entry 8).

To assess the scope and applicability of the optimized methodology, a series of aryl halides, encompassing unsubstituted and substituted aryl iodides, bromides, and chlorides bearing a variety of functional groups, were subjected to the reaction conditions (Table 2). The methodology proved robust, affording butyl cinnamate products in good to excellent yields across all tested substrates. A clear trend in halide reactivity was observed, with aryl iodides exhibiting the highest reactivity, followed by aryl bromides, and aryl chlorides requiring prolonged reaction times to achieve comparable conversions. This trend is consistent with the expected oxidative addition rates to the catalytic species. The influence of electronic effects was also investigated, revealing that electron-withdrawing substituents on the aryl ring facilitated the reaction, likely due to enhanced oxidative addition, while electron-donating groups retarded it. Notably, in the case of dihaloarenes, the reaction demonstrated exceptional chemoselectivity, selectively activating C–I and C–Br bonds in preference to C–Cl bonds (Table 2, entries 18 and 21). This selectivity is highly advantageous for synthetic applications where the chlorine functionality must be

Table 2 The scope of synthesis of butyl cinnamate *via* the Mizoroki–Heck C–C coupling reaction catalyzed by [Fe_3O_4@triazole-Schiff-base-Pd(0)]

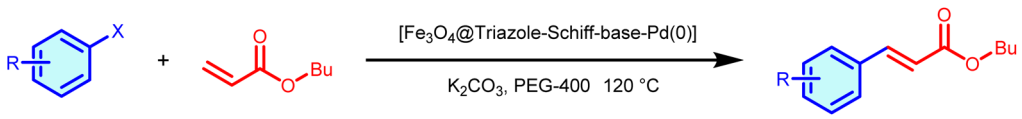

Entry	Aryl halide	Product	Time (min)	Yield[a,b] (%)	TON	TOF (min^{-1})	Melting point (°C)
1	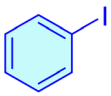	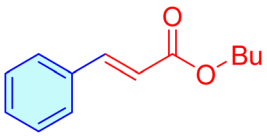	25	98	11 676	467.04	Oil[41]
2	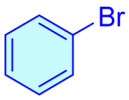	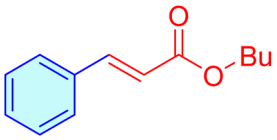	45	96	11 566	257.02	Oil[41]
3	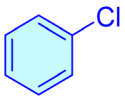	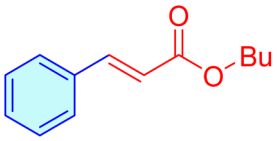	160	91	10 963	68.52	Oil[41]
4	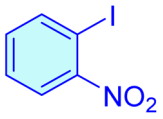	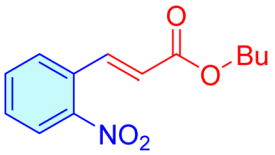	25	99	11 927	477.08	62–64 (ref. 42)
5	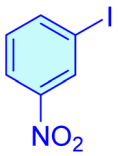	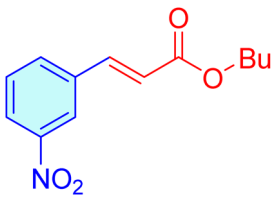	30	99	11 927	397.56	53–55 (ref. 43)
6	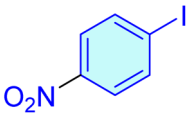	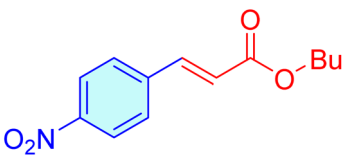	15	99	11 927	795.13	58–63 (ref. 41)
7	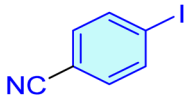	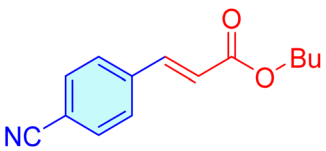	20	98	11 807	590.35	39–42 (ref. 41)
8	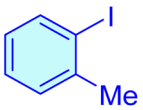	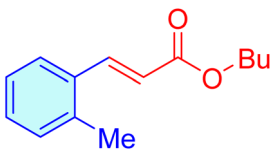	50	93	11 204	224.08	Oil[43]
9	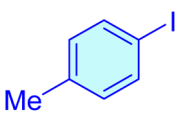	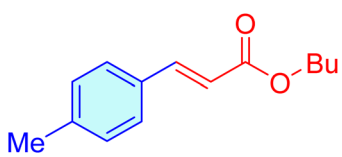	35	96	11 566	330.45	Oil[41]

Table 2 (*Contd.*)

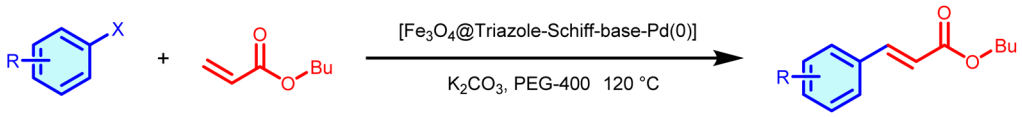

Entry	Aryl halide	Product	Time (min)	Yield[a,b] (%)	TON	TOF (min^{-1})	Melting point (°C)
10	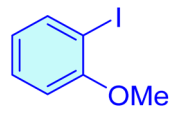	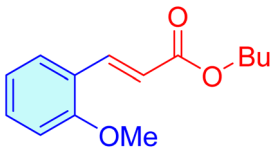	105	87	10 481	99.82	Oil[41]
11	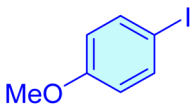	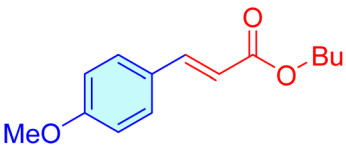	85	93	11 204	131.82	Oil[41]
12	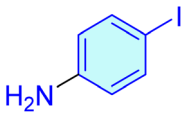	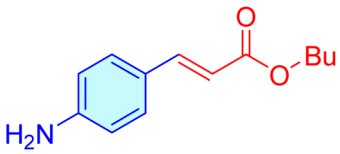	110	83	10 000	90.90	Oil[44]
13	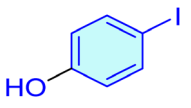	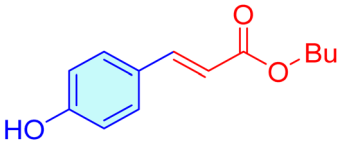	95	89	10 722	112.87	74–76 (ref. 45)
14	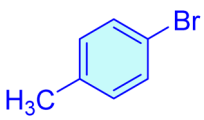	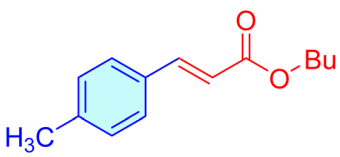	70	89	10 722	153.18	Oil[41]
15	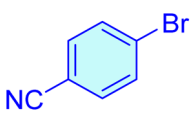	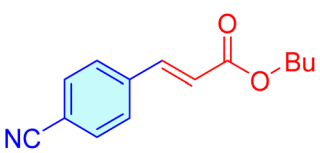	20	96	11 566	587.31	39–42 (ref. 41)
16	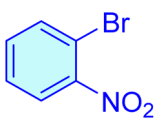	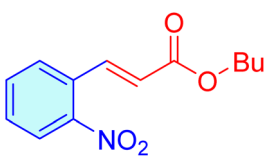	25	96	11 566	462.65	62–64 (ref. 42)
17	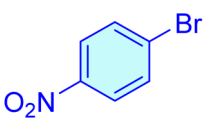	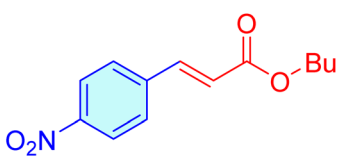	20	97	11 686	584.33	58–63 (ref. 41)
18	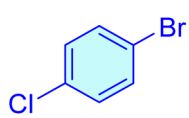	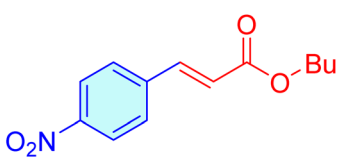	60	92	11 084	184.73	Oil[41]

Table 2 (*Contd.*)

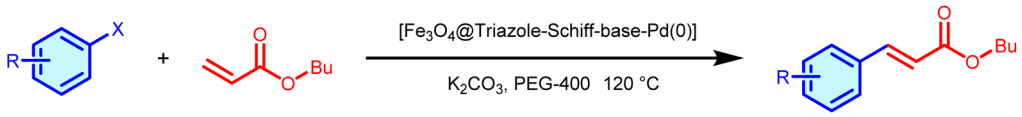

Entry	Aryl halide	Product	Time (min)	Yield[a,b] (%)	TON	TOF (min^{-1})	Melting point (°C)
19	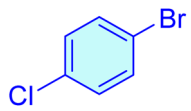	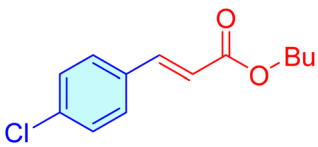	110	95	11 445	104.05	58–63 (ref. 41)
20	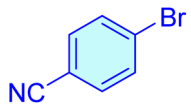	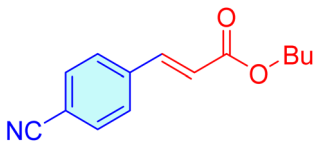	120	93	11 204	93.37	39–42 (ref. 46)
21	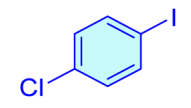	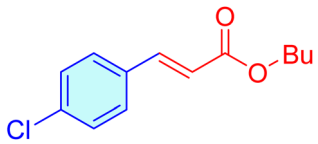	25	96	11 566	462.65	Oil[41]

[a] Isolated yield. [b] Conditions: aryl halide (1.0 mmol), butylacrylate (1 mmol) and the [Fe_3O_4@triazole-Schiff-base-Pd(0)] catalyst (5 mg) in PEG-400 (3 mL) at 120 °C.

retained, enabling selective coupling at the more reactive halide sites. Finally, to confirm the practical applicability and scalability of the optimized method, a gram-scale experiment was successfully performed. The reaction between iodobenzene and butyl acrylate, conducted at a 30 mmol scale, efficiently yielded the desired product in 95% within only 40 min, highlighting the method's high efficiency and robustness for larger-scale synthesis.

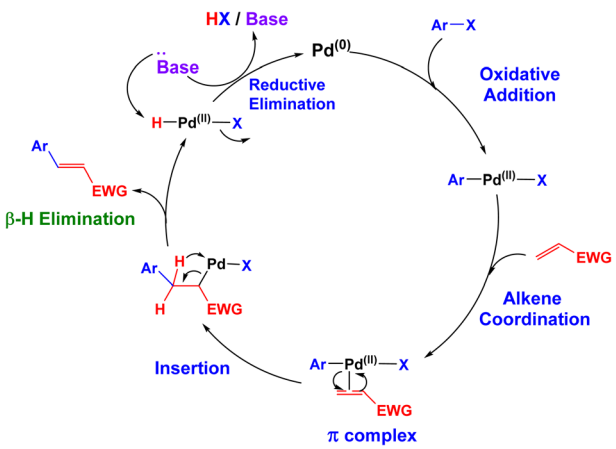

Scheme 2 Possible mechanism for synthesis of butyl cinnamate *via* the Mizoroki–Heck C–C coupling reaction catalyzed by [Fe_3O_4@triazole-Schiff-base-Pd(0)].

The proposed mechanism for the Mizoroki–Heck cross-coupling reaction over the [Fe_3O_4@triazole-Schiff-base-Pd(0)] catalyst is outlined in Scheme 2. The reaction initiates with the oxidative addition of aryl halide to a Pd(0) catalyst, generating a Pd(II) intermediate. Subsequently, the activated alkene coordinates to the palladium center, forming a π-complex. This is followed by a migratory insertion, where the aryl group inserts across the alkene double bond. The resulting alkylpalladium(II) species then undergoes β-hydride elimination, leading to the formation of the desired alkene product and a Pd(II)-hydride complex. Finally, reductive elimination of HX in the presence of the base regenerates the Pd(0) catalyst, completing the catalytic cycle.[47]

3.3. Reusability of the catalyst

The development of sustainable catalytic processes necessitates heterogeneous catalysts with high recyclability and stable active sites, especially when employing precious metals. These attributes are intrinsically linked: effective recycling hinges on minimizing active site loss or deactivation. Addressing challenges such as metal leaching and structural degradation is crucial for creating robust, reusable catalysts that enhance both economic and environmental viability.[48] To evaluate these critical properties, we conducted a comprehensive reusability study, encompassing catalyst recovery, hot filtration, and leaching tests. To assess catalyst reusability, the optimized model reaction was conducted across multiple reaction cycles.

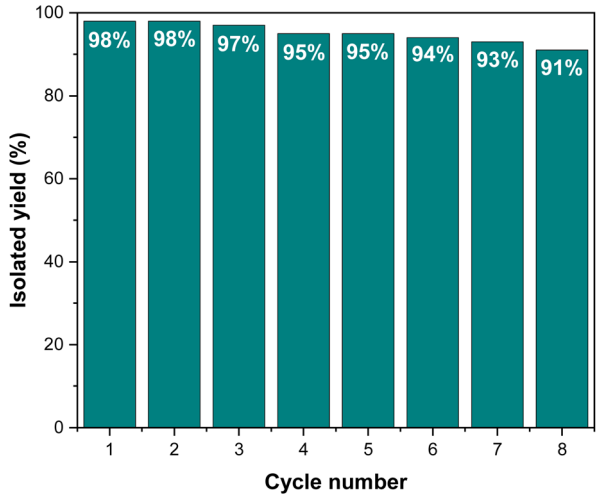

Fig. 9 The reusability of the [Fe_3O_4@triazole-Schiff-base-Pd(0)] complex in the model reaction of butyl cinnamate synthesis.

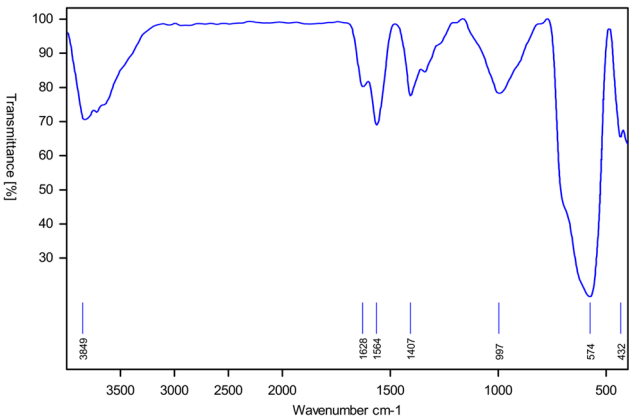

Fig. 10 FT-IR spectra of the recycled catalyst.

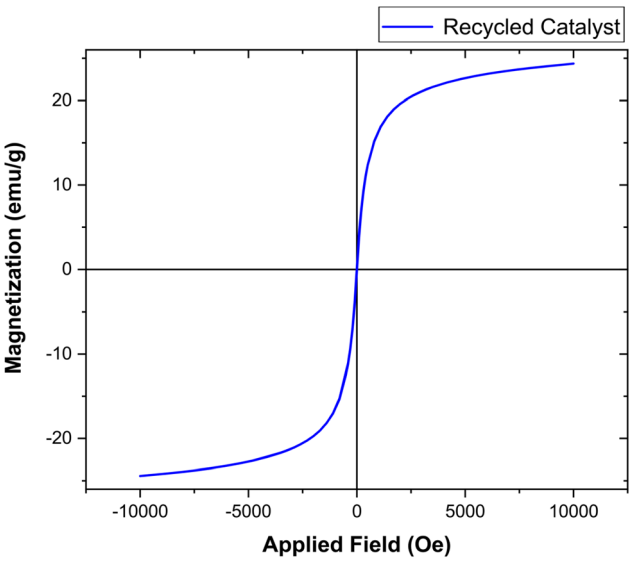

Fig. 11 VSM analysis of the recycled catalyst.

Upon completion of each cycle, the catalyst was isolated *via* the procedure described in the Experimental section. The recovered catalyst was subjected to rigorous washing with ethyl acetate, water, and ethanol, followed by drying at 80 °C. Subsequently, the catalyst was employed in subsequent reaction cycles. Over eight consecutive cycles, the catalyst exhibited remarkable stability, demonstrating minimal activity loss (Fig. 9). These results confirm the robust reusability and recyclability of the synthesized catalyst under the established optimized conditions.

The structural stability of the [Fe_3O_4@triazole-Schiff-base-Pd(0)] catalyst after multiple reaction cycles was rigorously evaluated using FT-IR, VSM, and ICP-OES analyses. The consistent FT-IR spectral pattern observed after eight cycles (Fig. 10) confirms the exceptional chemical stability and excellent recyclability of the catalyst. Additionally, VSM analysis (Fig. 11) showed that the M_s value of the spent catalyst was approximately 24.91 emu g^{-1}, indicating no significant decrease compared to the fresh catalyst. Furthermore, ICP-OES analysis revealed that the Pd content in the spent catalyst was 1.63 × 10^{-3} mol g^{-1}, which is very similar to that of the fresh catalyst, thereby providing strong evidence for the catalyst's stability throughout the reaction and recycling processes.

3.4. Leaching and the hot filtration test

The heterogeneous nature of the catalyst was further confirmed through a hot filtration test. Given the high viscosity of PEG-400, the reaction was conducted in ethanol. At half the reaction time of the model synthesis, the catalyst was removed *via* magnetic separation, yielding a 64% product conversion. Subsequent continuation of the reaction for an additional 4 h, under catalyst-free conditions, showed no significant increase in product conversion. This observation definitively establishes the catalyst's heterogeneous character. Furthermore, ICP-OES analysis of the filtrate demonstrated the absence of detectable palladium in the mixture. This result demonstrates the robust stability of the catalytic species anchored to the catalyst surface, indicating negligible leaching during the reaction.

3.5. Comparison study of catalytic activity

In recent years, various catalytic approaches have been developed for the Mizoroki–Heck C–C coupling reaction due to its crucial role in organic synthesis. However, a comparison between [Fe_3O_4@triazole-Schiff-base-Pd(0)] and the most effective methods documented in the literature reveals several drawbacks of conventional catalysts (Table 3). Many traditional catalysts depend on expensive, toxic, and phosphine-based ligands, with most being homogeneous and therefore non-reusable. Moreover, these homogeneous catalysts typically require high-cost metals such as palladium, iridium, rhodium, and ruthenium, extended reaction times, hazardous reagents or solvents, and additional purification steps. In contrast, [Fe_3O_4@triazole-Schiff-base-Pd(0)] presents a more sustainable solution. It functions effectively under eco-friendly conditions, achieving high yields within short reaction times. Additionally, its synthesis involves inexpensive, green reagents and ligands

Table 3 Comparison of the [Fe_3O_4@triazole-Schiff-base-Pd(0)] catalytic activity in synthesis of butyl cinnamate *via* the Mizoroki–Heck C–C coupling reaction

Entry	Catalyst	Time (min)	Yield (%)	Reference
1	$PdBr_2$-bis(N-heterocyclic carbene)	1440	99	49
2	Cyclometallated Pd(II) complex	25	97	50
3	Pd(II)–SBA-16	60	97	51
4	Bis(oxamato)palladate(II)	180	94	52
5	Fe_3O_4@MCM-41@Pd(0)–P2C	20	94	53
6	Spent automotive catalyst (s, containing Rh, Pd and Pt nanoparticles)	240	100	54
7	$[\{IrCl(cod)\}_2]$	24	71	55
8	(SP-5-41)-[1,3-Bis(2,4,6-trimethylphenyl)-2-imidazolidinylidene]dichloro [[2-(1-methylethoxy-κO)phenyl]methylene-κC]ruthenium	720	82	56
9	SiO_2–Rh^0	600	82	57
10	[Fe_3O_4@triazole-Schiff-base-Pd(0)]	25	98	This work

through a straightforward and scalable process while exhibiting minimal metal leaching. These benefits make it a highly promising, efficient, and environmentally friendly alternative to traditional catalytic methods.

4 Conclusions

In conclusion, a novel, magnetically recoverable palladium(0) Schiff base nanocomposite was synthesized *via* a facile post-synthetic modification. The resulting catalyst, comprising a magnetite core functionalized with a Schiff base ligand for palladium coordination, demonstrated effective performance as a reusable heterogeneous catalyst. Comprehensive characterization confirmed successful synthesis and structural integrity. FT-IR validated the ligand immobilization, XRD revealed high crystallinity, and FE-SEM and TEM confirmed uniform, spherical nano-sized particles. TGA indicated robust thermal stability up to 200 °C, while EDX, ICP-OES, elemental mapping, and VSM analyses substantiated the anticipated elemental composition and superparamagnetic properties. The [Fe_3O_4@-triazole-Schiff-base-Pd(0)]catalyst exhibited exceptional catalytic activity in the Mizoroki–Heck C–C coupling reaction, efficiently synthesizing butyl cinnamates from aryl halides and butyl acrylate in PEG-400 at 120 °C, achieving high yields. Notably, the catalyst displayed excellent reusability with minimal palladium leaching, demonstrating its stability and practical applicability. These results highlight the potential of this nanomagnetic palladium catalyst for a range of catalytic applications.

Data availability

The authors declare that all the data are available within the paper.

Author contributions

Asma Ahmad Nashawi and Jawza A. Almutairi: characterization of the catalyst and laboratory studies. Fatimah Mohammed Alshamsan: writing the original draft and laboratory studies. Yassin T. H. Mehdar: conceptualization, analysis, laboratory studies, review of the draft, acquiring research funding and supervision. Hussein Eledum and Ahmed Mohajja Alshammari: conceptualization, analysis, software and review/editing.

Conflicts of interest

The authors declare that they have no competing interests.

Acknowledgements

The authors are thankful to Princess Nourah Bint Abdulrahman University for financially supporting this work through the Researchers Supporting Project Number PNURSP2025R892.

References

1 S. Jagtap, Heck Reaction—State of the Art, *Catalysts*, 2017, 7, 267, DOI: 10.3390/catal7090267.
2 S. Vásquez-Céspedes, R. C. Betori, M. A. Cismesia, J. K. Kirsch and Q. Yang, Heterogeneous Catalysis for Cross-Coupling Reactions: An Underutilized Powerful and Sustainable Tool in the Fine Chemical Industry?, *Org. Process Res. Dev.*, 2021, **25**, 740–753, DOI: 10.1021/acs.oprd.1c00041.
3 K. M. Korch and D. A. Watson, Cross-Coupling of Heteroatomic Electrophiles, *Chem. Rev.*, 2019, **119**, 8192–8228, DOI: 10.1021/acs.chemrev.8b00628.
4 A. Biffis, P. Centomo, A. Del Zotto and M. Zecca, Pd Metal Catalysts for Cross-Couplings and Related Reactions in the 21st Century: A Critical Review, *Chem. Rev.*, 2018, **118**, 2249–2295, DOI: 10.1021/acs.chemrev.7b00443.
5 Q. Yang, N. R. Babij and S. Good, Potential Safety Hazards Associated with Pd-Catalyzed Cross-Coupling Reactions, *Org. Process Res. Dev.*, 2019, **23**, 2608–2626, DOI: 10.1021/acs.oprd.9b00377.
6 P. Devendar, R.-Y. Qu, W.-M. Kang, B. He and G.-F. Yang, Palladium-Catalyzed Cross-Coupling Reactions: A Powerful Tool for the Synthesis of Agrochemicals, *J. Agric. Food Chem.*, 2018, **66**, 8914–8934, DOI: 10.1021/acs.jafc.8b03792.

7 A. Kumar, G. K. Rao, S. Kumar and A. K. Singh, Formation and role of palladium chalcogenide and other species in Suzuki-Miyaura and heck C-C coupling reactions catalyzed with palladium(II) complexes of organochalcogen ligands: realities and speculations, *Organometallics*, 2014, **33**, 2921–2943, DOI: **10.1021/om4007196**.

8 M. Ashraf, M. S. Ahmad, Y. Inomata, N. Ullah, M. N. Tahir and T. Kida, Transition metal nanoparticles as nanocatalysts for Suzuki, Heck and Sonogashira cross-coupling reactions, *Coord. Chem. Rev.*, 2023, **476**, 214928, DOI: **10.1016/j.ccr.2022.214928**.

9 A. Modak, J. Mondal, V. K. Aswal and A. Bhaumik, A new periodic mesoporous organosilica containing diimine-phloroglucinol, Pd(ii)-grafting and its excellent catalytic activity and trans-selectivity in C–C coupling reactions, *J. Mater. Chem.*, 2010, **20**, 8099, DOI: **10.1039/c0jm01180k**.

10 A. Koranne, S. Turakhia, V. K. Jha, S. Gupta, R. Ravi, A. Mishra, A. K. Aggarwal, C. K. Jha, N. Dheer and A. K. Jha, The Mizoroki–Heck reaction between in situ generated alkenes and aryl halides: cross-coupling route to substituted olefins, *RSC Adv.*, 2023, **13**, 22512–22528, DOI: **10.1039/D3RA03533F**.

11 L. Jin, J. Qian, N. Sun, B. Hu, Z. Shen and X. Hu, Pd-Catalyzed reductive heck reaction of olefins with aryl bromides for Csp 2 –Csp 3 bond formation, *Chem. Commun.*, 2018, **54**, 5752–5755, DOI: **10.1039/C8CC02571A**.

12 K. Hong, M. Sajjadi, J. M. Suh, K. Zhang, M. Nasrollahzadeh, H. W. Jang, R. S. Varma and M. Shokouhimehr, Palladium Nanoparticles on Assorted Nanostructured Supports: Applications for Suzuki, Heck, and Sonogashira Cross-Coupling Reactions, *ACS Appl. Nano Mater.*, 2020, **3**, 2070–2103, DOI: **10.1021/acsanm.9b02017**.

13 L. Djakovitch and K. Koehler, Heck Reaction Catalyzed by Pd-Modified Zeolites, *J. Am. Chem. Soc.*, 2001, **123**, 5990–5999, DOI: **10.1021/ja001087r**.

14 L. Huang, Heterogeneity in Heck Reactions with Heterogeneous Precatalysts, *Curr. Org. Chem.*, 2018, **22**, 1022–1038, DOI: **10.2174/1385272822666180129143614**.

15 I. P. Beletskaya and A. V. Cheprakov, in *Modern Heck Reactions*, 2014, ch. 9, pp. 355–478, DOI: **10.1039/9781782620259-00355**.

16 M. Nasrollahzadeh, Advances in magnetic nanoparticles-supported palladium complexes for coupling reactions, *Molecules*, 2018, **23**, 2532, DOI: **10.3390/molecules23102532**.

17 K. Sarkar, M. Nandi, M. Islam, M. Mubarak and A. Bhaumik, Facile Suzuki coupling over ortho-metalated palladium(II) complex anchored on 2D-hexagonal mesoporous organosilica, *Appl. Catal., A*, 2009, **352**, 81–86, DOI: **10.1016/j.apcata.2008.09.033**.

18 R. Schlögl, *Heterogeneous Catalysis*, American Chemical Society, Washington, DC, USA, 2015, DOI: **10.1002/anie.201410738**.

19 Q. Zhang, X. Yang and J. Guan, Applications of Magnetic Nanomaterials in Heterogeneous Catalysis, *ACS Appl. Nano Mater.*, 2019, **2**, 4681–4697, DOI: **10.1021/acsanm.9b00976**.

20 V. Polshettiwar, R. Luque, A. Fihri, H. Zhu, M. Bouhrara and J. M. Basset, Magnetically recoverable nanocatalysts, *Chem. Rev.*, 2011, **111**, 3036–3075, DOI: **10.1021/cr100230z**.

21 D. Wang and D. Astruc, Fast-Growing Field of Magnetically Recyclable Nanocatalysts, *Chem. Rev.*, 2014, **114**, 6949–6985, DOI: **10.1021/cr500134h**.

22 Y. Zou, Z. Sun, Q. Wang, Y. Ju, N. Sun, Q. Yue, Y. Deng, S. Liu, S. Yang, Z. Wang, F. Li, Y. Hou, C. Deng, D. Ling and Y. Deng, Core-Shell Magnetic Particles: Tailored Synthesis and Applications, *Chem. Rev.*, 2025, **125**, 972–1048, DOI: **10.1021/acs.chemrev.4c00710**.

23 O. A. Mawlid, H. H. Abdelhady and M. S. El-Deab, Recent Advances in Magnetic Nanoparticle-Based Heterogeneous Catalysts for Efficient Biodiesel Production: A Review, *Energy Fuels*, 2024, **38**, 20169–20195, DOI: **10.1021/acs.energyfuels.4c03555**.

24 P. Kumar and P. Gupta, Halloysite-Based Magnetic Nanostructures for Diverse Applications: A Review, *ACS Appl. Nano Mater.*, 2023, **6**, 13824–13868, DOI: **10.1021/acsanm.3c02573**.

25 V. K. Juyal, A. Pathak, M. Panwar, S. C. Thakuri, O. Prakash, A. Agrwal and V. Nand, Schiff base metal complexes as a versatile catalyst: a review, *J. Organomet. Chem.*, 2023, **999**, 122825, DOI: **10.1016/j.jorganchem.2023.122825**.

26 A. Soroceanu and A. Bargan, Advanced and Biomedical Applications of Schiff-Base Ligands and Their Metal Complexes: A Review, *Crystals*, 2022, **12**, 1436, DOI: **10.3390/cryst12101436**.

27 C. Boulechfar, H. Ferkous, A. Delimi, A. Djedouani, A. Kahlouche, A. Boublia, A. S. Darwish, T. Lemaoui, R. Verma and Y. Benguerba, Schiff bases and their metal complexes: a review on the history, synthesis, and applications, *Inorg. Chem. Commun.*, 2023, **150**, 110451, DOI: **10.1016/j.inoche.2023.110451**.

28 S. Rezayati, A. Ramazani, S. Sajjadifar, H. Aghahosseini and A. Rezaei, Design of a Schiff Base Complex of Copper Coated on Epoxy-Modified Core-Shell MNPs as an Environmentally Friendly and Novel Catalyst for the One-Pot Synthesis of Various Chromene-Annulated Heterocycles, *ACS Omega*, 2021, **6**, 25608–25622, DOI: **10.1021/acsomega.1c03672**.

29 M. S. S. Adam, A. Taha, M. M. Mostafa, F. Ullah and M. M. Makhlouf, ZnO-TiO2 Nanoparticles Coated by the Dioxomolybdenum (VI) bis-Schiff Base Complex for Catalytic Oxidation of Sulfides, *ACS Appl. Nano Mater.*, 2023, **6**, 8515–8528, DOI: **10.1021/acsanm.3c00885**.

30 W. Li, K. Wang, J. Huang, X. Liu, D. Fu, J. Huang, Q. Li and G. Zhan, M x O y –ZrO 2 (M = Zn, Co, Cu) Solid Solutions Derived from Schiff Base-Bridged UiO-66 Composites as High-Performance Catalysts for CO 2 Hydrogenation, *ACS Appl. Mater. Interfaces*, 2019, **11**, 33263–33272, DOI: **10.1021/acsami.9b11547**.

31 Y. Wei, B. Han, X. Hu, Y. Lin, X. Wang and X. Deng, Synthesis of Fe3O4 nanoparticles and their magnetic properties, *Procedia Eng.*, 2012, **27**, 632–637, DOI: **10.1016/j.proeng.2011.12.498**.

32 K. M. Khan, S. Siddiqui, M. Saleem, M. Taha, S. M. Saad, S. Perveen and M. I. Choudhary, Synthesis of triazole Schiff

bases: Novel inhibitors of nucleotide pyrophosphatase/phosphodiesterase-1, *Bioorg. Med. Chem.*, 2014, **22**, 6509–6514, DOI: 10.1016/j.bmc.2014.08.032.

33 F. Rafiee and S. Hasani, The synthesis of Fe3O4@SiO2-NNO-CuII nanocatalyst and investigation of its application in the synthesis of imidazo[1,2-a]pyridines, *Results Chem.*, 2024, **11**, 101790, DOI: 10.1016/j.rechem.2024.101790.

34 Z. H. Chohan and M. Hanif, Synthesis and characterization of biologically active new Schiff bases containing 3-functionalized 1,2,4-triazoles and their zinc(II) complexes: crystal structure of 4-bromo-2-[(E)-(1H-1,2,4-triazol-3-ylimino)- methyl]phenol, *Appl. Organomet. Chem.*, 2011, **25**, 753–760, DOI: 10.1002/aoc.1833.

35 V. A. J. Silva, P. L. Andrade, M. P. C. Silva, A. D. Bustamante, L. De Los Santos Valladares and J. A. Aguiar, Synthesis and characterization of Fe3O4 nanoparticles coated with fucan polysaccharides, *J. Magn. Magn. Mater.*, 2013, **343**, 138–143, DOI: 10.1016/j.jmmm.2013.04.062.

36 A. Mazaheri and M. Bostanian, Synthesis and characterization of a novel functionalized magnetic Fe3O4 as a nanocatalyst for synthesis and antibacterial activities of 2-amino-3-phenylsulfonyl-4-aryl-4H-benzo[h]chromens derivatives and theoretical study on the mechanism using a DFT Meth, *Res. Chem. Intermed.*, 2020, **46**, 2327–2350, DOI: 10.1007/s11164-020-04094-y.

37 I. D. Inaloo, S. Majnooni, H. Eslahi and M. Esmaeilpour, Nickel(II) Nanoparticles Immobilized on EDTA-Modified Fe3O4@SiO2 Nanospheres as Efficient and Recyclable Catalysts for Ligand-Free Suzuki-Miyaura Coupling of Aryl Carbamates and Sulfamates, *ACS Omega*, 2020, **5**, 7406–7417, DOI: 10.1021/acsomega.9b04450.

38 V. Jeevanantham, D. Tamilselvi, K. Rathidevi, S. R. Bavaji and P. Neelakandan, Green formulation of palladium nanoparticles on photocatalytic behavior of fabric dyes removal and its antibacterial assay, *Biomass Convers. Biorefin.*, 2024, **14**, 20939–20948, DOI: 10.1007/s13399-023-04179-9.

39 A. Ghasemi-Ghahsareh, J. Safaei-Ghomi and H. S. Oboudatian, Supported l-tryptophan on Fe3O4@SiO2 as an efficient and magnetically separable catalyst for one-pot construction of spiro[indene-2,2′-naphthalene]-4′-carbonitrile derivatives, *RSC Adv.*, 2022, **12**, 1319–1330, DOI: 10.1039/d1ra07654j.

40 F. Mohammadi, A. Esrafili, M. Kermani and M. Behbahani, Application of modified magnetic nanoparticles with amine groups as an efficient solid sorbent for simultaneous removal of 2,4-dichlorophenoxyacetic acid and 2-methyl-4-chlorophenoxyacetic acid from aqueous solution: optimization and modeling, *J. Iran. Chem. Soc.*, 2018, **15**, 421–429, DOI: 10.1007/s13738-017-1243-5.

41 M. Nikoorazm, A. Ghorbani-Choghamarani, N. Noori and B. Tahmasbi, Palladium 2-mercapto-N-propylacetamide complex anchored onto MCM-41 as efficient and reusable nanocatalyst for Suzuki, Stille and Heck reactions and amination of aryl halides, *Appl. Organomet. Chem.*, 2016, **30**, 843–851, DOI: 10.1002/aoc.3512.

42 S. A. A. Alavi G, M. A. Nasseri, M. Kazemnejadi, A. Allahresani and M. Hussainzadeh, NiFe2O4@SiO2@ZrO2/SO42-/Cu/Co nanoparticles: a novel, efficient, magnetically recyclable and bimetallic catalyst for Pd-free Suzuki, Heck and C-N cross-coupling reactions in aqueous media, *New J. Chem.*, 2021, **45**, 7741–7757, DOI: 10.1039/d0nj06208a.

43 X. Li, X. Gong, Z. Li, H. Chang, W. Gao and W. Wei, Ligand- and copper-free Sonogashira and Heck couplings of (Het) aryl chlorides and bromides catalyzed by palladium nanoparticles supported on in situ generated Al(OH) 3, *RSC Adv.*, 2017, **7**, 2475–2479, DOI: 10.1039/C6RA25416K.

44 G. R. Rosa and D. S. Rosa, NCP pincer palladacycle as a phosphine-free catalyst precursor for the Heck–Mizoroki coupling of aryl halides, *RSC Adv.*, 2012, **2**, 5080, DOI: 10.1039/c2ra01261h.

45 S.-H. Huang, J.-R. Chen and F.-Y. Tsai, Palladium(II)/Cationic 2,2'-Bipyridyl System as a Highly Efficient and Reusable Catalyst for the Mizoroki-Heck Reaction in Water, *Molecules*, 2010, **15**, 315–330, DOI: 10.3390/molecules15010315.

46 A. Ghorbani-Choghamarani, B. Tahmasbi, N. Noori and S. Faryadi, Pd–S-methylisothiourea supported on magnetic nanoparticles as an efficient and reusable nanocatalyst for Heck and Suzuki reactions, *C. R. Chim.*, 2017, **20**, 132–139, DOI: 10.1016/j.crci.2016.06.010.

47 M. Mohammadi and A. Ghorbani-Choghamarani, L-Methionine-Pd complex supported on hercynite as a highly efficient and reusable nanocatalyst for C-C cross-coupling reactions, *New J. Chem.*, 2020, **44**, 2919–2929, DOI: 10.1039/C9NJ05325E.

48 M. Miceli, P. Frontera, A. Macario and A. Malara, Recovery/reuse of heterogeneous supported spent catalysts, *Catalysts*, 2021, **11**, 591, DOI: 10.3390/catal11050591.

49 M. V. Baker, D. H. Brown, P. V. Simpson, B. W. Skelton and A. H. White, Palladium complexes of o-xylyl-linked alkoxybenzimidazolin-2-ylidenes: interesting structural conformations and application as pre-catalysts, *Dalton Trans.*, 2009, 7294, DOI: 10.1039/b908613g.

50 A. Naghipour, M. Sayadi, A. Sedghi, S. J. Sabounchei, H. Babaee and B. Notash, A comparative study of palladium-based coordination compounds with bidentate (N,N, P,P and P,O) ligands; design, synthesis, X-ray structural, catalytic activity and DFT studies, *Inorg. Chim. Acta*, 2021, **515**, 120039, DOI: 10.1016/j.ica.2020.120039.

51 M. Niakan, Z. Asadi and M. Masteri-Farahani, A covalently anchored Pd(II)-Schiff base complex over a modified surface of mesoporous silica SBA-16: an efficient and reusable catalyst for the Heck-Mizoroki coupling reaction in water, *Colloids Surf., A*, 2018, **551**, 117–127, DOI: 10.1016/j.colsurfa.2018.04.066.

52 F. R. Fortea-Pérez, M. Julve, E. V. Dikarev, A. S. Filatov and S.-E. Stiriba, Synthesis and structural characterization of well-defined bis(oxamato)palladate(II) precatalysts for Suzuki and Heck reactions, *Inorg. Chim. Acta*, 2018, **471**, 788–796, DOI: 10.1016/j.ica.2017.12.012.

53 M. Nikoorazm, F. Ghorbani, A. Ghorbani-Choghamarani and Z. Erfani, Synthesis and characterization of a Pd(0) Schiff base complex anchored on magnetic nanoporous MCM-41 as a novel and recyclable catalyst for the Suzuki and Heck reactions under green conditions, *Chin. J. Catal.*, 2017, **38**, 1413–1422, DOI: **10.1016/S1872-2067(17)62865-1**.

54 E. Mieczyńska, A. Gniewek and A. M. Trzeciak, Spent automotive three-way catalysts towards CC bond forming reactions, *Appl. Catal., A*, 2012, **421–422**, 148–153, DOI: **10.1016/j.apcata.2012.02.012**.

55 T. Koike, X. Du, T. Sanada, Y. Danda and A. Mori, Iridium-Catalyzed Mizoroki–Heck-Type Reaction of Organosilicon Reagents, *Angew. Chem., Int. Ed.*, 2003, **42**, 89–92, DOI: **10.1002/anie.200390061**.

56 N. Suzuki, K. Watanabe, C. Takahashi, Y. Takeoka and M. Rikukawa, Ruthenium-catalyzed Olefin Metathesis in Water using Thermo-responsive Diblock Copolymer Micelles, *Curr. Org. Chem.*, 2023, **27**, 1347–1356, DOI: **10.2174/1385272827666230911115809**.

57 R. Trivedi, S. Roy, M. Roy, B. Sreedhar and M. L. Kantam, Catalysis of the Heck-type reaction of alkenes with arylboronic acids by silica-supported rhodium: an efficient phosphine-free reusable catalytic protocol, *New J. Chem.*, 2007, **31**, 1575, DOI: **10.1039/b706904a**.